Journal of
Nanoscience and Nanotechnology
Vol. 10, 7149–7153, 2010

Effect of Surface Related Organic Vibrational Modes in Luminescent Upconversion Dynamics of Rare Earth Ions Doped Nanoparticles

Yu Wang[1, 2, 3], Szymon Smolarek[1], Xianggui Kong[3, *], Wybren Jan Buma[1], Albert Manfred Brouwer[1], and Hong Zhang[1, *]

[1] *van't Hoff Institute for Molecular Sciences, University of Amsterdam, Nieuwe Achtergracht 166, 1018 WV Amsterdam, The Netherlands*
[2] *Graduate School of Chinese Academy of Sciences, Beijing 100039, P. R. China*
[3] *Changchun Institute of Optics, Fine Mechanics and Physics, Chinese Academy of Sciences, 3888 Eastern South Lake Road, Changchun 130033, P. R. China*

Physical and chemical properties of nanoparticles are known to be subject to the surface factors. For their biological/biomedical applications, typically, surface of the nanoparticles has to be modified which inevitably affects their performance. In this work we have studied the interaction between the surface related organic vibrational modes and the luminescent centers—rare earth ions—in one of the most efficient luminescence upconversion nanosystems—$NaYF_4$. Specifically, the surface quenching centers, the surface related luminescent centers, as well as the role of shell properties, are investigated spectroscopically. Our results demonstrate that the surface related high-frequency vibrational modes can be critical to the spectral properties of the nanosystems once the surface is not well separated from the discrete luminescent centers.

Keywords: Upconversion Nanoparticles, Surface Effect, Core/Shell, Organic Vibrational Modes.

1. INTRODUCTION

Interaction between inorganic nanoparticles and their surface related organic molecules can alter significantly the physical and chemical properties of the nanoparticles and therefore is key to the application of the nanoparticles, especially in the biological/biomedical field. On the other hand, upconversion nanoparticles, typically rare earth ions doped ones (e.g., $NaYF_4$ [1–4]) are regarded as of great potential as luminescence labels for imaging, therapy and detection, etc[5–10] because of their unique advantages, such as low photobleaching, multicolor labeling, deep penetration of excitation light (IR) in human tissues and IR-photon upconversion can be easily realized by an economic CW diode laser. Yet, approaches from different aspects have been developed to improve the upconversion efficiency: host material, lattice structure, doping concentration, etc. Lower symmetry and lower phonon energy of the crystal lattice are beneficial for the upconversion emission since vibrational energy coupling with the transition of rare earth ions promotes non-radiative relaxation. Sensitizer-acceptor co-doping and using sensitizers, such as Yb^{3+} ion, are proven to increase upconversion efficiency, since the former diminishes the phonon-assistant non-radiative channels and the latter can significant enhance the absorption cross section of the IR irradiation.

To study the effect of the surface related organic vibrational modes[11] on the spectroscopic properties of rare earth ions in upconversion nanoparticles, we have designed a series of core/shell structural nanoparticles of various thickness of the homogeneous shell. Coating a homogeneous shell outside a core is considered to be an efficient route to enhance the upconversion luminescence of the nanoparticles.[12, 13] In general it is either modifying/annulling the surface defects and/or shielding high frequency vibrating modes from outside. In this work we focus on the effect of the thickness of the α-$NaYF_4$ shell around Yb^{3+}, Er^{3+}@α-$NaYF_4$ particles on the upconversion dynamics to illustrate the role of homogeneous coating.

2. EXPERIMENTAL DETAILS

The synthesis was in general similar to those previous reported.[14–16] Briefly, rare earth trifluoroacetates

*Authors to whom correspondence should be addressed.

 1533-4880/2010/10/7149/005 doi:10.1166/jnn.2010.2878

$((CF_3COO)_3RE \cdot 3H_2O)$ were prepared by dissolving the rare earth oxides in trifluoroacetic acid (CF_3COOH), then drying at 60 °C. A mixture of designated molar ratio of trifluoroacetate salts powder ($Na^+/RE^{3+} = 1/1$, $Y^{3+}/Yb^{3+}/Er^{3+} = 78/20/2$, mol/mol) were dissolved in 10 mL oleic acid (OA), 10 ml oleylamine (OM) and 20 ml octadecene (ODE) then passed through a filter to get rid of the residues. The mixture was then vigorous stirred in a three neck flask and heated to 110 °C and maintained at this temperature to remove the residual water and oxygen for more than 30 min. The flask was purged periodically with dry argon gas for protection from oxidation. At this point the solution was totally clear with a slight orange color. Then the mixture was heated slowly to 250 °C in the presence of argon atmosphere. After 2 hrs reaction at 250 °C, the product was cooled down to room temperature. A little amount of the product was taken out as the reference, the rest was separated into six equal shares. Each part of the product we obtained was reheated to 250 °C again under vigorous stirring and the protection of dry argon gas. Different amounts of shell precursor (equal molar of sodium trifluoroacetate and yttrium trifluoroacetate dissolved in OA/OM/ODE mixture) were slowly added into the reaction systems immediately when the temperature got to 250 °C. All of the followed reactions were allowed to continue for another 1 h. Every final mixture was cool down rapidly to room temperature, precipitated with ethanol and isolated via centrifugation for three times. The resulting nanocrystals were dried in vacuum at 60 °C for a minimum of 24 hrs. According to the increasing amount of shell materials we denote the samples as S1, S2, S3, S4, S5 and S6.

Structure characterization was performed via SEM images obtained at a field emission scanning electron microscope (FE-SEM, Hitachi, S-4800), where a small drop of the sample re-dispersed in hexane was deposited on silicon substrate and air dried. The upconversion emission spectra were acquired using a Jobin-Yvon LabRam Raman spectrometer system equipped with holographic gratings of 1800 and 600 grooves/mm and a Peltier air-cooled CCD detector. A 980 nm CW laser diode was used for optical excitation and the beam was focused to a spot size of approximately 0.2 mm in diameter. The lifetimes of the $^4S_{3/2}$ and $^4F_{9/2}$ states for Er^{3+} was measured with a 500 MHz Tektronix digital oscilloscope under excitation of 980 nm light pulses from an *ns* optical parametric oscillator.

3. RESULTS AND DISCUSSION

In this experiment six α-$NaYF_4$: Yb^{3+}, Er^{3+}@α-$NaYF_4$ core/shell structure samples were synthesized, the schematic illustration of the six samples is given in Scheme 1. The α-$NaYF_4$: Yb^{3+}, Er^{3+} cores remain the same size, and the only difference among them is the shell thickness, which could be controlled in shell growing period. Figure 1 shows the SEM images of the six samples. The average particle sizes were 8.8 nm (S1), 10.9 nm (S2), 12.8 nm (S3), 15.1 nm (S4), 17.5 nm (S5), 20.0 nm (S6), respectively. For reference, a SEM image of the naked core nanoparticles is also given in Figure 1, from which the size of the core was determined to be 6.0 nm with narrow distribution. The large size differences of the samples S1 to S6 makes the size and shape distribution of the samples negligible.

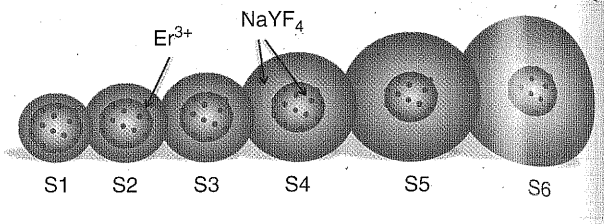

Scheme 1. Schematic illustration of the structure of the samples S1 to S6.

The integrated intensities of upconversion emission spectra of the six α-$NaYF_4$ nanoparticle samples are shown in Figure 2, where the excitation is set at 980 nm from a CW diode laser and the excitation power density is about 60 W/cm^2. Compared with S1, the upconversion emission intensity increased from ~20 times (S2) to ~160 times (S6). This trend can be rationalized by the fact that the smaller a sample is, the greater the surface will be to the properties of the nanoparticle. For example, the one of ~6 nm in size, the surface area is more than 60%, which means that more than 60% of the rare earth ions locate in the surface thin layer. The absorbed energy is subject to non-radiative relaxation caused by surface defects and high-frequency vibrational modes of the coupled organic molecules, and thus leads to weak emission.

Surprisingly, spectral structural change versus the shell thickness reveals non-monotonous nature, as is shown in Figure 3. Along with the thickness increase the red/green ratio increases from 8.5 (S1) to 12.0 (S3), and then decreases from 12.0 (S3) to 9.5 (S6). To disentangle this puzzle we have to consider the complex upconversion mechanism that occurs in rare earth ions. In Er^{3+}, for example, several population routes co-exist for the $^4F_{9/2}$ level. In our previous work[12] it was proven that cross relaxation can not be neglected when the Er^{3+} concentration is over 2%. Strong cross relaxation favors strong red emission. When the first layer of homogeneous shell was grown at the surface of the nanoparticles, a significant amount of non-radiative centers located at the surface of the $NaYF_4$: Yb^{3+}, Er^{3+} nanoparticles were eliminated due to the shielding effect of the $NaYF_4$ shell, the cross relaxation process could be enhanced, which resulted in the increase of red/green ratio. The process described above is defined as the first stage. On the other hand, when the shell continued growing in the second stage, the surface and emission centers would be separated more and

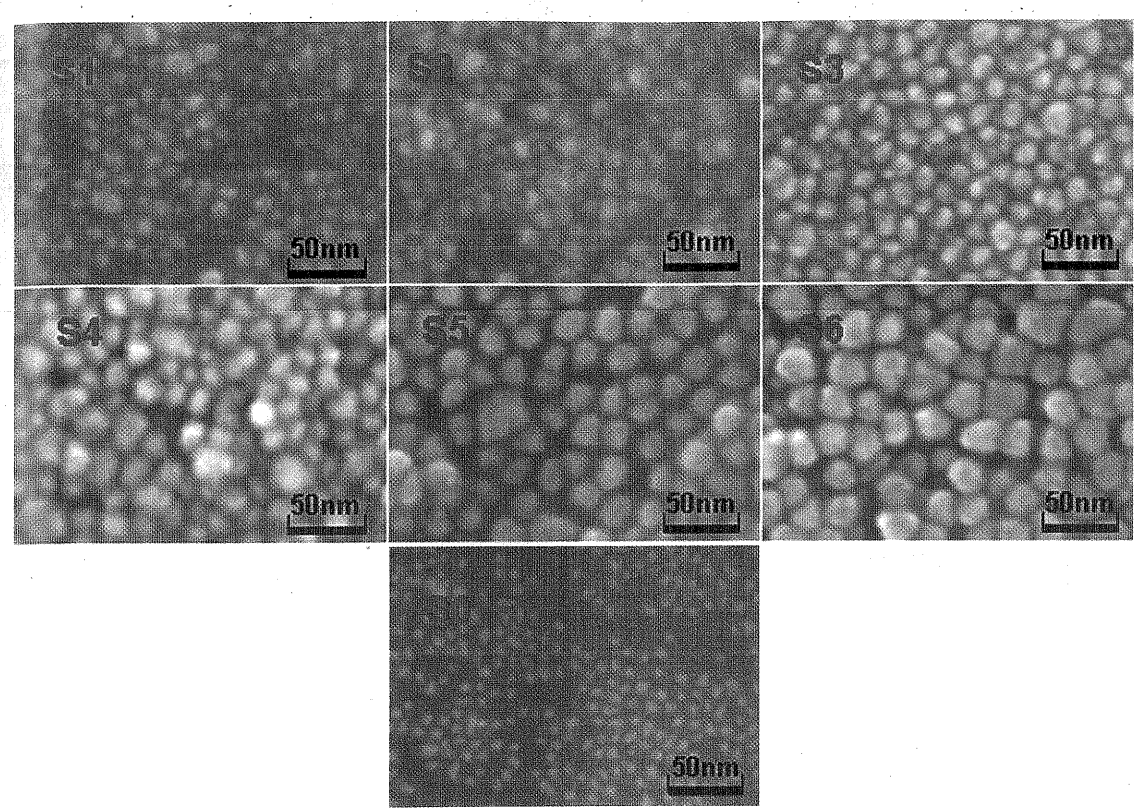

Fig. 1. SEM images of S1–S6. S0 is the naked core nanoparticles.

more in space by the shell, which weakened the interaction between high-frequency organic vibration modes and optical transitions in emitting ions, and thus the population for the red emission is less. This might be one explanation for the decrease of the red/green ratio at the second stage.

Considering the upconversion mechanism (excited state absorption (ESA) or energy transfer upconversion (ETU)) the intensity of the visible output will be proportional to some power (n) of the infrared excitation power density.

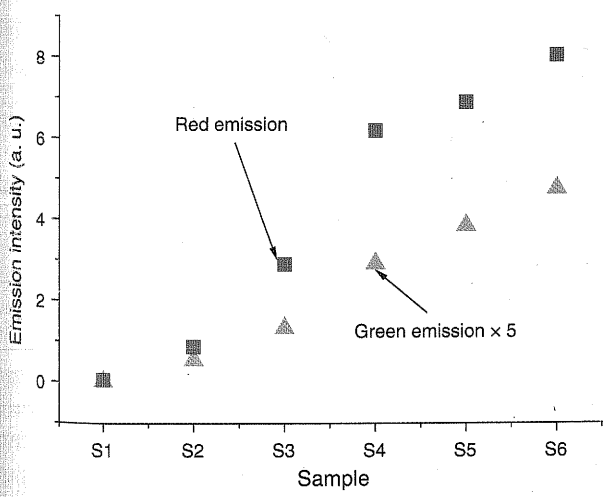

Fig. 2. Green and red integrated upconversion emissions of the six samples under the excitation power density of about 60 W/cm^2. The green emission band (520–560 nm) is enlarged by 5 times.

In our experiments n varied from 3.37 to 2.90 for red emission and from 3.09 to 2.51 for green emission with the increase of the shell thickness, as shown in Figure 4. This phenomenon manifested itself the involvement of processes other than ETU and/or ESA which should lead to n not over 2. But considering the relatively high doping concentration of Er^{3+} (2 mol%) cross relaxation ($^2H_{11/2} \rightarrow {}^4F_{9/2}$ vs. $^4I_{11/2} \rightarrow {}^4F_{9/2}$) should occur here,[17] which lead to $n > 2$. The population of $^4F_{7/2}$ from the three photon energy level ($^4G_{11/2}$) might be another reason. This assignment seems against the observation that in core/shell

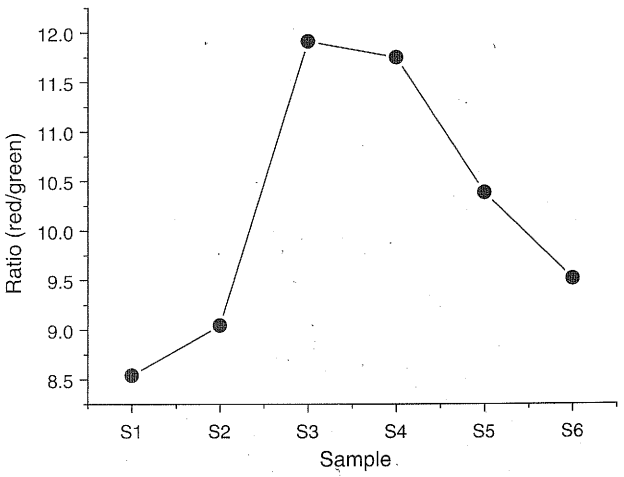

Fig. 3. The intensity ratio of red/green of the six samples under IR excitation with the power density of 60 W/cm^2.

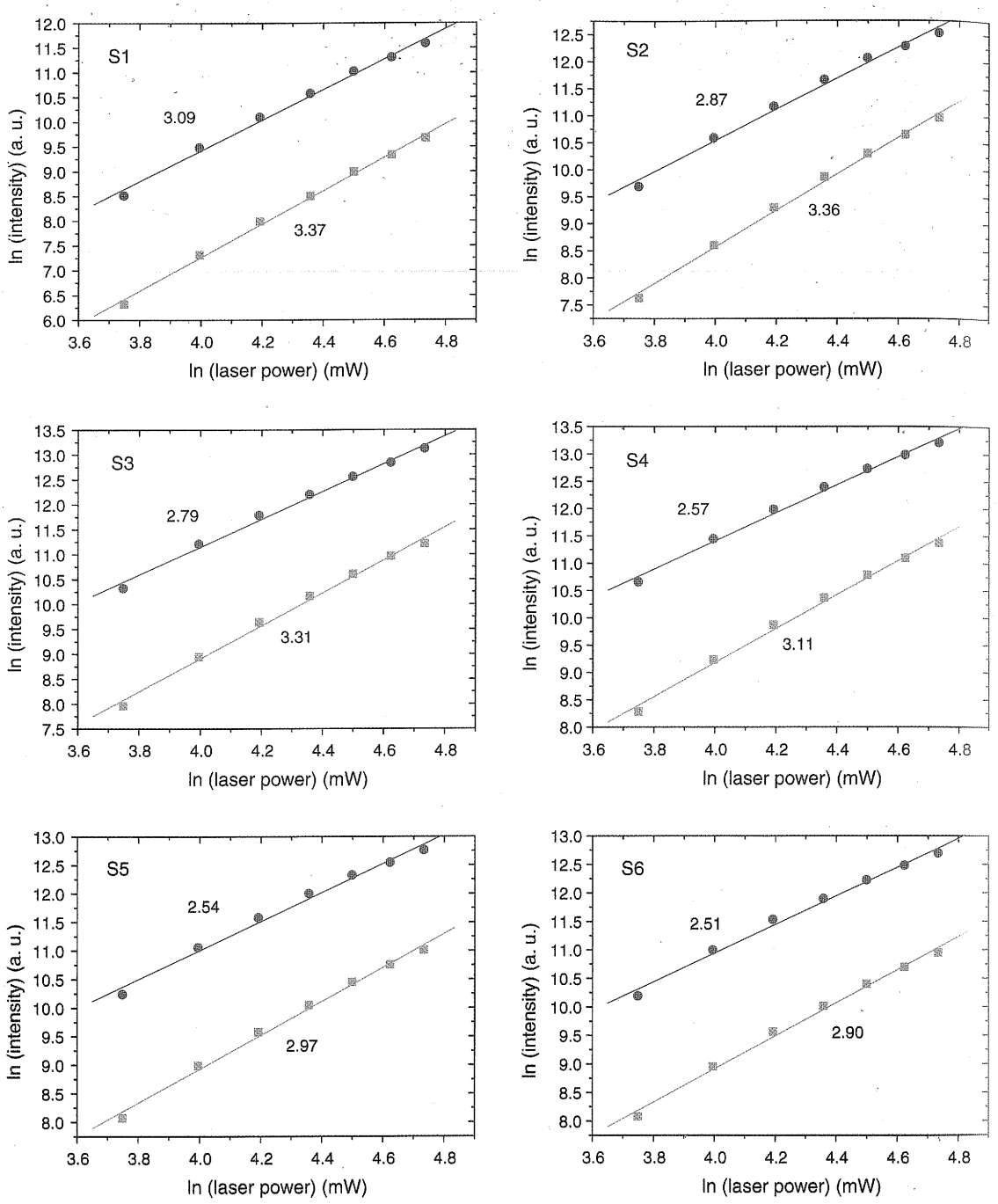

Fig. 4. Logarithmic plots of the integrated intensities of the upconversion emissions from levels $^2H_{11/2}/^4S_{3/2}$ and $^4F_{9/2}$ to $^4I_{15/2}$ under 980 nm CW laser excitation.

structures n was much closer to 2 in thicker shell samples, where, compared to the core nanoparticles, the high frequency vibrational modes brought in by the surface organic groups would be much less. The non-radiative relaxation efficiency decreased when the shell got thicker, hence the non-radiative relaxation from $^4G_{11/2}$ to $^4F_{7/2}$ decreased. More population of $^4G_{11/2}$ contributed to ultraviolet radiation, rather than to $^4F_{7/2}$ via non-radiative relaxation.

The time evolution of the green ($^4S_{3/2}$–$^4I_{15/2}$) and red ($^4F_{9/2}$–$^4I_{15/2}$) upconversion luminescence of the six samples of core/shell nanoparticles are collected. All the green and red luminescence decay curves of the samples were very close to exponential form, which means that all the local environments of the emission centers were nearly the same. For a 6 nm-diameter-core-nanoparticle, there are only less than 700 lattice cells and only 2% of them have emission centers. All curves can be well fitted with two components: one rises and one decays. It has to be realized that when a rise and a decay component coexist in luminescence kinetics, decay is always the longer one, even if

Table I. Rise and decay components of the green- and the red emissions of core–shell nanoparticles of different shell thickness.

	Green emission (545 nm)		Red emission (660 nm)	
	Rise lifetime (μs)	Average decay lifetime (μs)	Rise lifetime (μs)	Average decay lifetime (μs)
S1	8	73	40	113
S2	10	168	50	327
S3	13	200	78	440
S4	13	290	93	672
S5	13	345	106	850
S6	13	350	110	990

the population rate is faster.[12] Upconversion luminescence of rare earth ions is just one of such examples. Since the intermediate states that mediate the upconversion process, e.g., $^4I_{11/2}$ and $^4I_{13/2}$ have longer lifetimes than that of the upconversion emission states, e.g., $^4S_{3/2}$ (for green emission) and $^4F_{9/2}$ (for red emission), the rise components in our measurements are determined mainly by the lifetimes of the latter states, whereas the intermediate states, i.e., $^4I_{11/2}$ and/or $^4I_{13/2}$, are responsible to the decay components of the upconversion luminescence kinetics. Therefore the rise constant reflects mainly the nature of $^4I_{11/2}$ states in green emission and $^4I_{13/2}$ states in red emission, and the decay constant represents more the lifetime of the $^4S_{3/2}$ or $^4F_{9/2}$. From Table I it can be seen that for both the green and red emissions, the upconversion luminescence decay lifetime increased when the shell thickness increases. The same is true for the rise time constant of the red emission. The rise lifetime of green emission, however, remained constant after sample S3, which means that the aforementioned surface-related effects could be negligible in considering the vibrational relaxation dynamics of $^4I_{11/2}$ state.

4. CONCLUSIONS

From luminescence kinetics analysis it is clear that a large number of luminescent centers of the core nanoparticle are severely quenched, but can be recovered by homogeneous coating. Our results demonstrate that the surface-related high-frequency vibrational modes play an important role in the upconversion process. Coating a homogenous shell can alter the upconversion channels and thus can be used to manipulate the upconversion mechanism and further the upconversion luminescence spectra.

Acknowledgments: This work was supported by NSFC of China (60771051, 60601015, 10674132, 10874179 and 20603035), and exchange program between CAS of China and KNAW of the Netherlands.

References and Notes

1. N. Menyuk, K. Dwight, and F. Pinaud, *Appl. Phys. Lett.* 21, 159 (**1972**).
2. J. L. Sommerdijk and A. Bril, *Philips Tech. Rev.* 34, 1 (**1974**).
3. J. Zhao, Y. Sun, X. Kong, L. Tian, Y. Wang, L. Tu, J. Zhao, and H. Zhang, *J. Phys. Chem. B* 112, 15666 (**2008**).
4. Y. Sun, Y. Chen, L. Tian, Y. Yu, X. Kong, J. Zhao, and H. Zhang, *Nanotechnology* 18, 275609 (**2007**).
5. F. Van de Rijke, H. Zijlmans, S. Li, T. Vail, A. K. Raap, R. S. Niedbala, and H. J. Tanke, *Nat. Biotechnol.* 19, 273 (**2001**).
6. S. F. Lim, R. Riehn, W. S. Ryu, N. Khanarian, C. K. Tung, D. Tank, and R. H. Austin, *Nano Lett.* 6, 169 (**2006**).
7. L. Y. Wang and Y. D. Li, *Chem. Commun.* 24, 2557 (**2006**).
8. P. Zhang, W. Steelant, M. Kumar, and M. Scholfield, *J. Am. Chem. Soc.* 129, 4526 (**2007**).
9. P. Zhang, S. Rogelj, K. Nguyen, and D. Wheeler, *J. Am. Chem. Soc.* 128, 12410 (**2006**).
10. M. Nyk, R. Kumar, T. Y. Ohulchanskyy, E. J. Bergey, and P. N. Prasad, *Nano Lett.* 8, 3834 (**2008**).
11. L. Tian, Y. Sun, Y. Yu, X. Kong, and H. Zhang, *Chem. Phys. Lett.* 452, 188 (**2008**).
12. Y. Wang, L. Tu, J. Zhao, Y. Sun, X. Kong, and H. Zhang, *J. Phys. Chem. C* 113, 7164 (**2009**).
13. G. Yi and G. M. Chow, *Chem. Mater.* 19, 341 (**2007**).
14. J. C. Boyer, F. Vetrone, L. A. Cuccia, and J. A. Capobianco, *J. Am. Chem. Soc.* 128, 7444 (**2006**).
15. J. W. Stouwdam and F. C. J. M. van Veggel, *Langmuir* 20, 11763 (**2004**).
16. G. Yi and G. M. Chow, *Adv. Funct. Mater.* 16, 2324 (**2006**).
17. F. Liu, E. Ma, D. Chen, Y. Yu, and Y. Wang, *J. Phys. Chem. B* 110, 20843 (**2006**).

Received: 4 September 2009. Accepted: 30 October 2009.